研究成果の刊行物・別刷

Imaging Amyloid Pathology in the Living Brain

Nobuyuki Okamura[a,*], Shozo Furumoto[b], Hiroyuki Arai[c], Ren Iwata[d], Kazuhiko Yanai[a] and Yukitsuka Kudo[b]

[a]*Department of Pharmacology, Tohoku University School of Medicine, Sendai 980-8575, Japan,* [b]*Tohoku University Biomedical Engineering Research Organization (TUBERO), Sendai 980-8575, Japan,* [c]*Center for Asian Traditional Medicine, Department of Geriatrics and Gerontology, Tohoku University School of Medicine, Sendai 980-8574, Japan,* [d]*Division of Radiopharmaceutical Chemistry, Cyclotron and Radioisotope Center, Tohoku University, Sendai 980-8578, Japan*

Abstract: Progressive deposition of amyloid plaques in the brain, which begins before the appearance of cognitive decline, is an initiating event in the pathogenesis of Alzheimer's disease. Therefore, noninvasive detection of amyloid pathology is important for presymptomatic diagnosis and preventive therapy for Alzheimer's disease. Recent research advances have enabled the *in vivo* imaging of amyloid pathology in humans using nuclear medicine technology. Several amyloid-binding agents have been developed and evaluated by positron emission tomography (PET) and single photon emission computed tomography (SPECT) for their use as contrast agents. Available clinical evidence indicates that amyloid imaging enables the early diagnosis of Alzheimer's disease with high accuracy and suggests its usefulness for the prediction of progression to Alzheimer's disease in subjects with mild cognitive impairment and probably also in cognitively normal individuals. Another application of this technology is as a surrogate marker for monitoring brain amyloid. In this review, we describe recent progress in the development of amyloid imaging technology and human clinical trials.

Keywords: Amyloid, Alzheimer's disease, Positron emission tomography (PET), molecular imaging, senile plaque, neurofibrillary tangle.

INTRODUCTION

Alzheimer's disease (AD) is the most common cause of dementia in the elderly. The definitive diagnosis of AD relies on postmortem assessment, with characteristic pathological changes such as neuron death, senile plaques (SPs), and neurofibrillary tangles (NFTs). Currently, the amyloid cascade hypothesis is widely accepted to account for the pathogenesis of AD [1]. SP is mainly composed of amyloid β (Aβ), which is generated by proteolytic reaction of β and γ-secretase from the amyloid precursor protein (APP). In this hypothesis, the mismetabolism of APP is the initiating event in AD pathogenesis. Excessive generation of Aβ causes aggregation of Aβ and the formation of SPs, and this is followed by the formation of NFTs, neuron death, neurotransmitter deficit, and cognitive decline. If this hypothesis is correct, optimal therapeutic strategies for interrupting the disease process should be directed toward modifying the generation, clearance, and cytotoxicity of Aβ.

Early diagnosis and treatment of AD is important in maintaining the patient's activities of daily living as long as possible and preventing the patient from becoming bedridden. A notable feature of AD is a discrepancy between clinical symptoms and pathological findings in the brain (Fig. (1)). Even in the clinically early stage of dementia, a large amount of SP is already present in the brain [2, 3]. These changes in the brain probably start 10–20 years before clinical symptoms appear. Therefore, if the deposition of SPs in the brain can be measured noninvasively, subjects who are certain to develop AD (i.e., "preclinical AD") could be screened as candidates for preventive therapy.

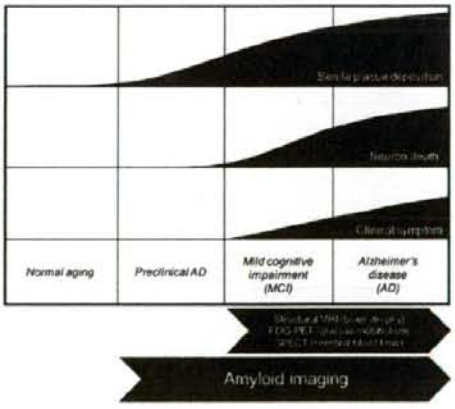

Fig. (1). Senile plaque deposition, neuron death and clinical symptom of Alzheimer's disease.

Recently, several imaging techniques, including positron emission tomography (PET), single photon emission computed tomography (SPECT), magnetic resonance imaging, and near-infrared imaging, have been developed for the noninvasive detection of SPs in AD patients. These techniques, recently classified as "amyloid imaging", are considered ideal for screening candidates for anti-amyloid therapy. PET is the most popular method for amyloid

*Address correspondence to this author at the Department of Pharmacology, Tohoku University School of Medicine, 2-1, Seiryo-machi, Aoba-ku, Sendai 980-8575, Japan; Tel: + 81-22-717-8058; Fax: +81-22-717-8060; E-mail: oka@mail.tains.tohoku.ac.jp

1573-4056/08 $55.00+.00

imaging, because of its advantages of high sensitivity, good spatial resolution, quantitative results, and ease of probe development.

DEVELOPMENT OF AMYLOID-IMAGING AGENTS

Recent advances in molecular imaging have enabled the noninvasive detection of amyloid deposits by PET or SPECT. For the high-contrast detection of amyloid deposits, imaging agents should have high binding affinity for Aβ fibrils and substantial permeability through the blood–brain barrier (BBB). Several amyloid-binding agents have been developed for the *in vivo* detection of amyloid deposits (Fig. (2)). The development of these agents started with the use of Congo red, which is commonly used for the histochemical staining of amyloid [4]. However, the BBB permeability of Congo red is limited because of its molecular size and electrostatic charge. Therefore, several Congo red derivatives have been developed with improved BBB permeability without reduced binding to amyloid [5-8]. Chrysamine-G is the first Congo red derivative that has been examined as an *in vivo* amyloid-imaging probe. However, entry of this compound into the brain is limited. Other derivatives, including BSB, ISB, and methoxy-X04, have also been developed to improve the BBB permeability. BSB successfully visualizes brain amyloid deposits in APP-transgenic mice after intravenous administration of the compound. However, this compound has insufficient BBB permeability for it to be useful as a clinical PET tracer. The first successful amyloid imaging agent to have been administered to humans is 2-(1-{6-[(2-[^{18}F]fluoroethyl)(methyl)amino]-2-naphthyl}ethylidene)malononitrile ([^{18}F]FDDNP) [9]. One of the characteristics of this agent is its ability to bind both SPs and NFTs in the AD brain. In addition, this compound is extremely lipophilic; therefore, it can penetrate the BBB more easily than previously reported compounds [10]. Interestingly, this compound binds to the same site in Aβ fibrils as non-steroidal anti-inflammatory drugs (NSAIDs) do. Therefore, this agent enables us to determine the occupancy rate of NSAIDs and experimental drugs in SPs [11]. Other candidate amyloid-imaging agents include thioflavin-T derivatives [12, 13]. N-methyl-[^{11}C]2-(4'-methylaminophenyl)-6-hydroxybenzothiazole ([^{11}C]PIB) is one such derivative and is currently the most successful amyloid-imaging agent. This compound shows high binding affinity for Aβ fibrils and SPs in AD brain homogenates, in contrast to low binding affinity for NFTs [14]. After intravenous administration, this agent shows high BBB permeability and rapid washout from normal brain tissue. Other amyloid-imaging agents, such as IMPY, stilbene, benzofuran, and acridine orange derivatives, have also been explored for use as PET and SPECT imaging probes [15-19]. The iodinated agent IMPY has been explored as a SPECT

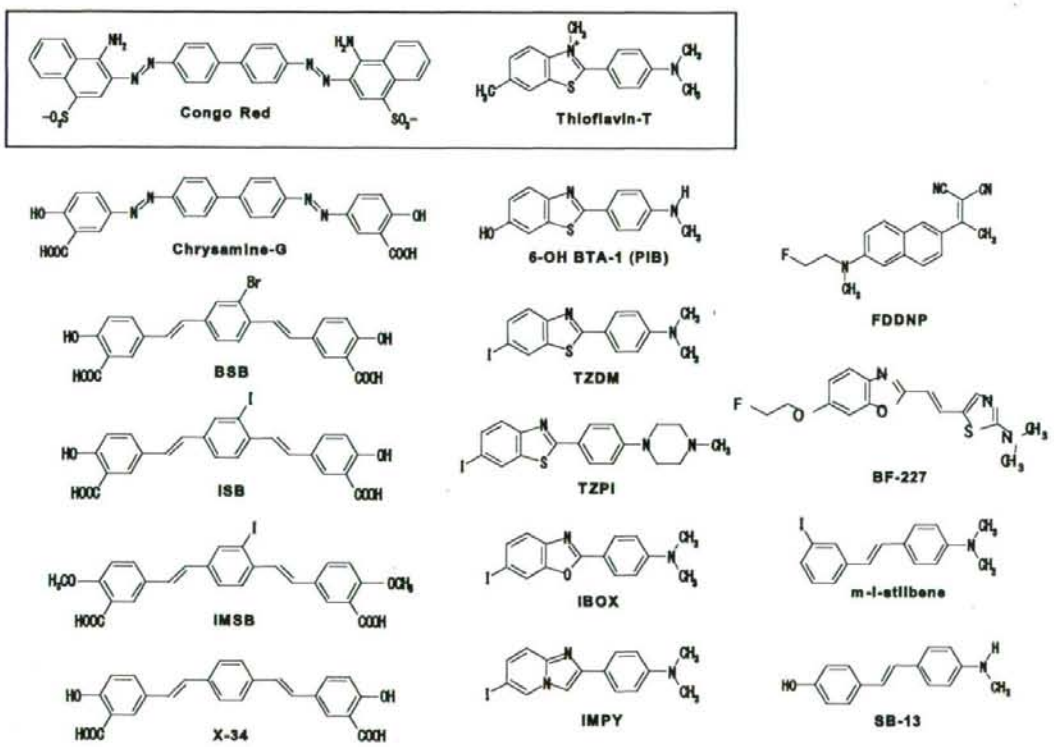

Fig. (2). Chemical structures of common imaging probes for amyloid plaques.

imaging agent and has been used in humans. Other iodinated agents are also under evaluation.

Benzoxazole derivatives are other possible amyloid-imaging agents [20-23]. Their chemical structures, binding affinities for Aβ fibrils, and pharmacokinetic data are summarized in Table 1. Most of these compounds show high binding affinity for both Aβ1-40 and Aβ1-42 fibrils. BF-191 and BF-208, which have halogens as substituents for amino groups, show low affinity for both Aβ1-40 and Aβ1-42 fibrils, suggesting that amino groups have a crucial role in binding to Aβ fibrils. All compounds have good BBB permeability. BF-227 shows faster washout from normal brain tissue than the other compounds [23, 24]. BF-227 distinctly stained SPs during the neuropathological staining of AD brain sections, and this staining pattern correlated well with Aβ immunostaining (Fig. (3)). Fluorescence microscopy revealed that this agent binds preferentially to SPs rather than NFTs. An acute and subacute toxicity study of BF-227 indicated sufficient safety for clinical use as a PET probe.

HUMAN PET STUDY

Human amyloid imaging was first studied using [^{18}F] FDDNP [9]. A [^{18}F]FDDNP PET study revealed regional accumulation of [^{18}F]FDDNP in the SP- and NFT-rich areas of the brain [25]. Global FDDNP-PET binding distinctly differentiated AD patients from normal subjects. FDDNP retention in the medial temporal lobes of subjects with mild cognitive impairment (MCI) was intermediate between levels in AD patients and normal control subjects. This finding is consistent with the observation in an autopsy study that the concentration of NFTs in the medial temporal lobes was intermediate between that in normally aging subjects and AD patients [26]. These binding characteristics indicate that this imaging agent is useful in tracing the progression of AD from the MCI stage. In addition, this agent has the potential to differentiate atypical prion disease from AD [27]. The weakness of this agent is the low signal-to-background ratio of the images, which is due to the considerable amount of nonspecific accumulation in normal brain tissue [28].

In comparison with [^{18}F]FDDNP, [^{11}C]PIB PET images differentiated AD patients from normal individuals more distinctly [29]. PIB retention was observed in the SP-rich neocortex of the brain but not in the NFT-rich medial temporal cortex, indicating that this agent binds selectively to SPs. A quantitative imaging method using PIB has already been validated [30, 31]. Over half the subjects with MCI also showed neocortical PIB accumulation to the same level as AD patients [32, 33]. Interestingly, MCI subjects who at clinical follow-up converted to AD showed higher PIB retention than subjects with non-progressive MCI, indicating that neocortical PIB retention is a marker for the prediction of progression to AD in the MCI stage [34]. A PIB-PET study in a nondemented population revealed elevated cortical retention of PIB in four nondemented persons [35]. These nondemented PIB-positive cases additionally showed an abnormality in the concentration of Aβ1-42 in cerebrospinal fluid, suggesting the presence of SPs in the absence of cognitive impairment [36]. There was a strong relationship between impaired memory performance and PIB binding in the nondemented population [37]. These findings suggest that amyloid imaging may be sensitive enough for the detection of a preclinical AD state. However, one should be careful when assessing abnormalities in the distribution of PIB, because PIB retention is also observed in cerebral amyloid angiopathy [38, 39]. Amyloid imaging may be useful as a surrogate marker for monitoring brain amyloid deposition during anti-amyloid therapy. However, longitudinal PIB-PET evaluation indicated relatively stable PIB retention after 2 years of follow-up in AD patients, suggesting that brain amyloid deposition reflected by PIB retention reaches a plateau at the early clinical stages of AD [40]. Therefore, therapy that retards the synthesis of Aβ (e.g., β- and γ-secretase inhibitors) should be started before the retention of amyloid-imaging tracers reaches a plateau.

The stilbene derivative SB-13 has also been used in a human PET study [41]. In a PET study, [^{11}C]SB-13 exhibited similar binding properties to PIB. For expanded use in clinical investigations, an ^{18}F-labeled stilbene derivative is under investigation.

A PET study using [^{11}C]BF-227 was performed at Tohoku University [23]. Neocortical retention of BF-227 was observed in an AD patient (Fig. (4)). A subject with MCI also showed cortical retention of BF-227. Interestingly, this subject was confirmed to progress to AD during the follow-up period, suggesting that cortical retention of BF-227 indicates a high risk of conversion to AD in MCI subjects. Several MCI subjects showed a distribution of BF-227 similar to that in normally aged subjects. All Alzheimer's patients and about 60% of MCI subjects showed an elevated standardized uptake value (SUV) ratio in the neocortical regions. Even in MCI subjects showing prominent retention of BF-227, the neocortical SUV ratio was below the mean value observed in AD patients. This finding suggests that MCI is a pathologically transitional state between normal aging and dementia, and that the amyloid deposition reflected by BF-227 retention does not reach a plateau in the MCI stage. Voxel-by-voxel analysis of BF-227 PET images demonstrated higher retention of BF-227 in the temporoparietal region in AD patients [23]. The pattern of distribution resembles the distribution of neuritic plaques in postmortem AD brains [42, 43]. Microscopic observation also indicates preferential binding of BF-227 to neuritic plaques in AD brain sections (Fig. (3)). In an *in vitro* binding experiment, BF-227 binding to Aβ increased linearly with increasing Aβ fibril formation [24]. For these reasons, BF-227 is considered to bind neuritic plaques selectively *in vivo*. A validation study is required to determine whether the retention of BF-227 in the neocortex accurately reflects the level of neuritic plaques rather than the level of diffuse plaques.

FUTURE DIRECTION OF PROBE DEVELOPMENT

The commercialization of ^{18}F-labeled agents or SPECT imaging agents is necessary for the wide clinical application of amyloid imaging. Because of the limited half-life of ^{11}C (20 min), the supply of ^{11}C-labeled PET agents is limited to facilities with an on-site cyclotron. ^{18}F-labeled agents are generally easier for routine clinical use because of the longer half-life of ^{18}F (110 min). Currently, several ^{18}F-labeled agents for amyloid imaging are under clinical evaluation. To

Table 1. Binding Affinity of Benzoxazole Derivatives for Aβ Fibrils and Brain Uptakes After Intravenous Administration in Normal Mice

Compounds	Chemical structure	Kd or Ki (nM)		Brain uptake (%ID/g)	
		Aβ1-40	Aβ1-42	2 min	30 min
BF-125	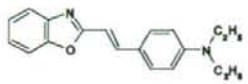	1.5 ± 0.76	4.9 ± 1.9	3.0 ± 0.87	3.0 ± 0.53
BF-133	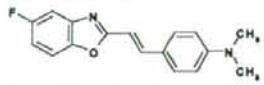	2.1 ± 1.1	3.4 ± 0.73	5.5 ± 0.40	3.8 ± 0.030
BF-140	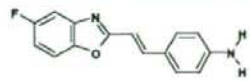	4.7 ± 2.2	2.1 ± 0.18	5.5 ± 0.60	1.1 ± 0.076
BF-145	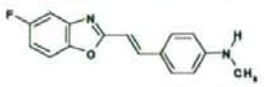	3.0 ± 0.46	4.5 ± 1.9	4.4 ± 1.80	1.6 ± 0.40
BF-168	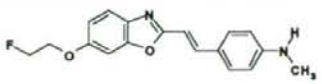	2.5 ± 2.3	6.4 ± 1.0	3.9 ± 0.22	1.6 ± 0.0071
BF-180	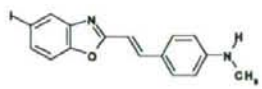	6.8 ± 1.4	10.6 ± 1.5	2.4 ± 0.52	1.8 ± 0.010
BF-185	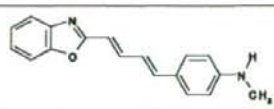	2.5 ± 2.3	14 ± 10	3.9 ± 0.49	3.8 ± 0.16
BF-191	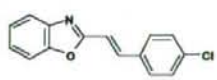	> 5000	> 5000	12 ± 0.26	1.7 ± 0.16
BF-208	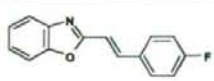	> 5000	> 5000	5.6 ± 0.64	0.28 ± 0.024
BF-227	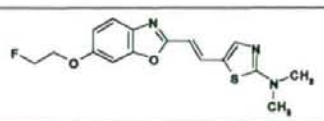	1.8 ± 0.42	4.3 ± 1.5	7.9 ± 0.18	0.54 ± 0.029

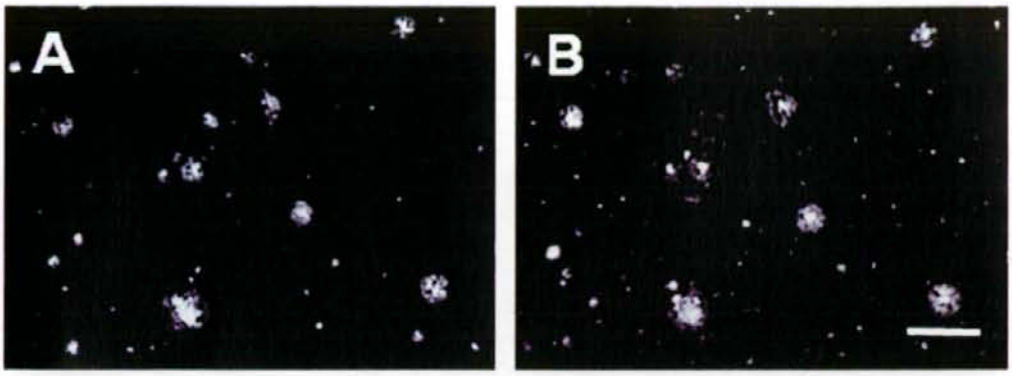

Fig. (3). Fluorescence microscopic images of senile plaques in Alzheimer's disease using BF-227 (A) and Aβ specific antibody 6F/3D (B) Bar = 100μm.

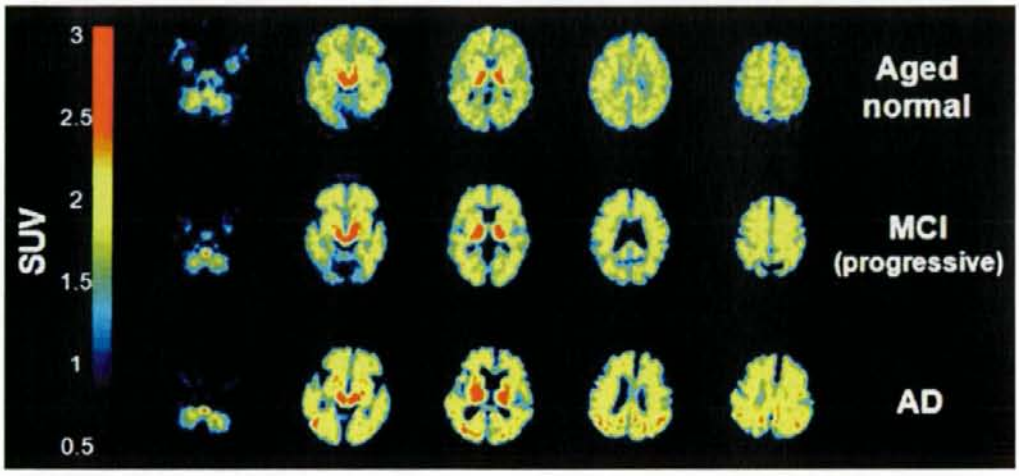

Fig. (4). Mean SUV images between 20 and 40 min post-injection of [^{11}C]BF-227 in aged normal, MCI and AD cases.

obtain a better understanding of the pathophysiology of AD, it is also necessary to visualize the distributions of Aβ pathology and tau pathology individually. However, no surrogate markers are available for evaluating the deposition of NFTs in the brain, because of the difficulty in developing a tau-specific imaging probe [44]. We previously introduced the novel compounds BF-126 and BF-170 as candidates for tau imaging [45]. In AD brain sections, BF-126 and BF-170 visualize NFTs, neuropil threads, and PHF-type neuritis distinctly. For clinical application, optimization of these compounds to reduce non-specific binding is in progress.

CONCLUSION

Several amyloid-imaging agents have been successfully developed for PET imaging. These agents displayed high binding affinity for Aβ fibrils and high BBB permeability. [^{11}C]PIB, [^{18}F]FDDNP, and [^{11}C]BF-227 displayed selective *in vivo* binding to amyloid in the brain and clearly differentiated early AD patients from normal populations. The development of ^{18}F-labeled agents or SPECT imaging agents is necessary for the wide application of amyloid imaging. The development of an NFT-specific imaging agent is also much needed. Amyloid imaging is currently the best method for the early and accurate diagnosis of AD and for monitoring amyloid pathology in the brain. This imaging technology and the forthcoming anti-amyloid therapy will cooperatively contribute to the prevention of dementia.

ACKNOWLEDGEMENTS

This study was partially supported by the Special Coordination Funds for Promoting Science and Technology, the Program for the Promotion of Fundamental Studies in Health Science of the National Institute of Biomedical Innovation, the Industrial Technology Research Grant

Program of the New Energy and Industrial Technology Development Organization (NEDO) of Japan, Health and Labour Sciences Research Grants for Translational Research from the Japanese Ministry of Health, Labour and Welfare, and a JST grant for research and education in molecular imaging.

DISCLOSURE STATEMENT

All authors have no conflict of interest.

REFERENCES

[1] Tanzi RE, Bertram L. Twenty years of the Alzheimer's disease amyloid hypothesis: a genetic perspective. Cell 2005; 120: 545-555.

[2] Goldman WP, Price JL, Storandt M, *et al.* Absence of cognitive impairment or decline in preclinical Alzheimer's disease. Neurology 2001; 56: 361-367.

[3] Price JL, Morris JC. Tangles and plaques in nondemented aging and "preclinical" Alzheimer's disease. Ann Neurol 1999; 45: 358-368.

[4] Klunk WE, Debnath ML, Pettegrew JW. Development of small molecule probes for the beta-amyloid protein of Alzheimer's disease. Neurobiol Aging 1994; 691-698.

[5] Klunk WE, Debnath ML, Pettegrew JW. Chrysamine-G binding to Alzheimer and control brain: autopsy study of a new amyloid probe. Neurobiol Aging 1995; 16: 541-548.

[6] Skovronsky DM, Zhang B, Kung MP, Kung HF, Trojanowski JQ, Lee VM. *In vivo* detection of amyloid plaques in a mouse model of Alzheimer's disease. Proc Natl Acad Sci USA 2000; 97: 7609-7614.

[7] Zhuang ZP, Kung MP, Hou C, *et al.* Radioiodinated styrylbenzenes and thioflavins as probes for amyloid aggregates. J Med Chem 2001; 44: 1905-1914.

[8] Klunk WE, Bacskai BJ, Mathis CA, *et al.* Imaging Abeta plaques in living transgenic mice with multiphoton microscopy and methoxy-X04, a systemically administered Congo red derivative. J Neuropathol Exp Neurol 2002; 61: 797-805.

[9] Shoghi-Jadid K, Small GW, Agdeppa ED, *et al.* Localization of neurofibrillary tangles and beta-amyloid plaques in the brains of living patients with Alzheimer disease. Am J Geriatr Psychiatry 2002; 10: 24-35.

[10] Agdeppa ED, Kepe V, Liu J, *et al.* Binding characteristics of radiofluorinated 6-dialkylamino-2-naphthylethylidene derivatives as positron emission tomography imaging probes for beta-amyloid plaques in Alzheimer's disease. J Neurosci 2001; 21: RC189.

[11] Agdeppa ED, Kepe V, Petri A, *et al. In vitro* detection of (S)-naproxen and ibuprofen binding to plaques in the Alzheimer's brain using the positron emission tomography molecular imaging probe 2-(1-[6-[(2-[(18)F]fluoroethyl)(methyl) amino]-2-naphthyl]ethylidene)malononitrile. Neuroscience 2003; 117: 723-730.

[12] Mathis CA, Wang Y, Klunk WE. Imaging beta-amyloid plaques and neurofibrillary tangles in the aging human brain. Curr Pharm Des 2004; 10: 1469-1492.

[13] Klunk WE, Wang Y, Huang GF, Debnath ML, Holt DP, Mathis CA. Uncharged thioflavin-T derivatives bind to amyloid-beta protein with high affinity and readily enter the brain. Life Sci 2001; 69: 1471-1484.

[14] Klunk WE, Wang Y, Huang GF, *et al.* The binding of 2-(4'-methylaminophenyl)benzothiazole to postmortem brain homogenates is dominated by the amyloid component. J Neurosci 2003; 23: 2086-2092.

[15] Kung MP, Hou C, Zhuang ZP, *et al.* IMPY: an improved thioflavin-T derivative for *in vivo* labeling of beta-amyloid plaques. Brain Res 2002; 956: 202-210.

[16] Kung HF, Kung MP, Zhuang ZP, *et al.* Iodinated tracers for imaging amyloid plaques in the brain. Mol Imaging Biol 2003; 5: 418-426.

[17] Ono M, Wilson A, Nobrega J, *et al.* ^{11}C-labeled stilbene derivatives as Abeta-aggregate-specific PET imaging agents for Alzheimer's disease. Nucl Med Biol 2003; 30: 565-571.

[18] Ono M, Kawashima H, Nonaka A, *et al.* Novel benzofuran derivatives for PET imaging of beta-amyloid plaques in Alzheimer's disease brains. J Med Chem 2006; 49: 2725-2730.

[19] Suemoto T, Okamura N, Shiomitsu T, *et al. In vivo* labeling of amyloid with BF-108. Neurosci Res 2004; 48: 65-74.

[20] Okamura N, Suemoto T, Shimadzu H, *et al.* Styrylbenzoxazole derivatives for *in vivo* imaging of amyloid plaques in the brain. J Neurosci 2004; 24: 2535-2541.

[21] Okamura N, Suemoto T, Shiomitsu T, *et al.* A novel imaging probe for *in vivo* detection of neuritic and diffuse amyloid plaques in the brain. J Mol Neurosci 2004; 24: 247-255.

[22] Furumoto S, Okamura N, Iwata R, Yanai K, Arai H, Kudo Y. Recent advances in the development of amyloid imaging agents. Curr Top Med Chem 2007; 7: 1773-1789.

[23] Kudo Y, Okamura N, Furumoto S, *et al.* 2-(2-[2-Dimethylaminothiazol-5-yl]ethenyl)-6- (2-[fluoro]ethoxy)benzoxazole: a novel PET agent for *in vivo* detection of dense amyloid plaques in Alzheimer's disease patients. J Nucl Med 2007; 48: 553-561.

[24] Okamura N, Furumoto S, Funaki Y, *et al.* Binding and safety profile of novel benzoxazole derivative for *in vivo* imaging of amyloid deposits in Alzheimer's disease. Geriatr Gerontol Int 2007 (in press)

[25] Small GW, Kepe V, Ercoli LM, *et al.* PET of brain amyloid and tau in mild cognitive impairment. N Engl J Med 2006; 355: 2652-2663.

[26] Petersen RC, Parisi JE, Dickson DW, *et al.* Neuropathologic features of amnestic mild cognitive impairment. Arch Neurol 2006; 63: 665-672.

[27] Boxer AL, Rabinovici GD, Kepe V, *et al.* Amyloid imaging in distinguishing atypical prion disease from Alzheimer disease. Neurology 2007; 69: 283-290.

[28] Bacskai BJ, Klunk WE, Mathis CA, Hyman BT. Imaging amyloid-beta deposits *in vivo*. J Cereb Blood Flow Metab 2002; 22: 1035-1041.

[29] Klunk WE, Engler H, Nordberg A, *et al.* Imaging brain amyloid in Alzheimer's disease with Pittsburgh Compound-B. Ann Neurol 2004; 55: 306-319.

[30] Price JC, Klunk WE, Lopresti BJ, *et al.* Kinetic modeling of amyloid binding in humans using PET imaging and Pittsburgh Compound-B. J Cereb Blood Flow Metab 2005; 25: 1528-1547.

[31] Lopresti BJ, Klunk WE, Mathis CA, *et al.* Simplified quantification of Pittsburgh Compound B amyloid imaging PET studies: a comparative analysis. J Nucl Med 2005; 46: 1959-1972.

[32] Rowe CC, Ng S, Ackermann U, *et al.* Imaging beta-amyloid burden in aging and dementia. Neurology. 2007; 68: 1718-1725.

[33] Kemppainen NM, Aalto S, Wilson IA, *et al.* PET amyloid ligand [^{11}C]PIB uptake is increased in mild cognitive impairment. Neurology 2007; 68: 1603-1606.

[34] Forsberg A, Engler H, Almkvist O, *et al.* PET imaging of amyloid deposition in patients with mild cognitive impairment. Neurobiol Aging 2007 (in press)

[35] Mintun MA, Larossa GN, Sheline YI, *et al.* [^{11}C]PIB in a nondemented population: potential antecedent marker of Alzheimer disease. Neurology 2006; 67: 446-452.

[36] Fagan AM, Mintun MA, Mach RH, *et al.* Inverse relation between *in vivo* amyloid imaging load and cerebrospinal fluid Abeta42 in humans. Ann Neurol 2006; 59: 512-519.

[37] Pike KE, Savage G, Villemagne VL, *et al.* Beta-amyloid imaging and memory in non-demented individuals: evidence for preclinical Alzheimer's disease. Brain 2007; 130: 2837-2844.

[38] Bacskai BJ, Frosch MP, Freeman SH, *et al.* Molecular imaging with Pittsburgh Compound B confirmed at autopsy: a case report. Arch Neurol 2007; 64: 431-434.

[39] Johnson KA, Gregas M, Becker JA, *et al.* Imaging of amyloid burden and distribution in cerebral amyloid angiopathy. Ann Neurol 2007; 62: 229-234.

[40] Engler H, Forsberg A, Almkvist O, *et al.* Two-year follow-up of amyloid deposition in patients with Alzheimer's disease. Brain 2006; 129: 2856-2866.

[41] Verhoeff NP, Wilson AA, Takeshita S, *et al.* In-vivo imaging of Alzheimer disease beta-amyloid with [^{11}C]SB-13 PET. Am J Geriatr Psychiatry 2004; 12: 584-595.

[42] Arnold SE, Hyman BT, Flory J, Damasio AR, Van Hoesen GW. The topographical and neuroanatomical distribution of neurofibrillary tangles and neuritic plaques in the cerebral cortex of patients with Alzheimer's disease. Cereb Cortex 1991; 1: 103-116.

[43] Cummings JL, Cole G. Alzheimer disease. JAMA 2002; 287: 2335-2338.

[44] Small GW, Agdeppa ED, Kepe V, Satyamurthy N, Huang SC, Barrio JR. *In vivo* brain imaging of tangle burden in humans. *J* Mol Neurosci 2002; 19: 323-327.

[45] Okamura N, Suemoto T, Furumoto S, *et al.* Quinoline and benzimidazole derivatives: candidate probes for *in vivo* imaging of tau pathology in Alzheimer's disease. *J* Neurosci 2005; 25: 10857-10862.

Received: December 5, 2007 Revised: December 7, 2007 Accepted: December 10, 2007

BJCP British Journal of Clinical Pharmacology

DOI:10.1111/j.1365-2125.2007.03063.x

In vivo visualization of donepezil binding in the brain of patients with Alzheimer's disease

Nobuyuki Okamura,[1] Yoshihito Funaki,[2] Manabu Tashiro,[3] Motohisa Kato,[1] Yoichi Ishikawa,[2] Masahiro Maruyama,[4] Hiroyasu Ishikawa,[5] Kenichi Meguro,[5] Ren Iwata[2] & Kazuhiko Yanai[1]

[1]Department of Pharmacology, Tohoku University Graduate School of Medicine, Sendai, [2]Division of Radiopharmaceutical Chemistry, Cyclotron and Radioisotope Center, Tohoku University, Sendai, [3]Division of Nuclear Medicine, Cyclotron and radioisotope centre, Tohoku University, Sendai, [4]Department of Geriatric and Complementary Medicine, Tohoku University Graduate School of Medicine, Sendai and [5]Department of Geriatric Behavioural Neurology, Tohoku University Graduate School of Medicine, Sendai, Japan

Correspondence
Dr Nobuyuki Okamura MD, PhD, Department of Pharmacology, Tohoku University School of Medicine, 2-1, Seiryo-machi, Aoba-ku, Sendai 980-8575, Japan.
Tel.: + 81 2 2717 8058;
Fax: + 81 2 2717 8060;
E-mail: oka@mail.tains.tohoku.ac.jp

Keywords
acetylcholinesterase, Alzheimer's disease, donepezil, positron emission tomography (PET)

Received
1 July 2007

Accepted
26 September 2007

Published *OnlineEarly*
7 December 2007

WHAT IS ALREADY KNOWN ABOUT THIS SUBJECT

- Deficit in central cholinergic neurotransmission is a consistent change associated with Alzheimer's disease (AD).
- Donepezil hydrochloride exhibits selective inhibition of acetylcholinesterase (AChE) and is widely used for the treatment of AD.
- The biodistribution of donepezil in the brain after administration is not precisely understood *in vivo*.
- There is no method to measure the amount of binding of orally administered donepezil to AChE.

WHAT THIS STUDY ADDS

- This study clearly visualizes the distribution of donepezil in human brain using [^{11}C]-donepezil and positron emission tomography.
- This study demonstrates prominent reduction of the donepezil binding site in the AD brain.
- This study provides methodology to measure the AChE binding occupancy of orally administered donepezil and provides a new surrogate marker for evaluation and prediction of response to donepezil treatment.

AIMS

The aims of this study were to visualize *in vivo* binding of donepezil to acetylcholinesterase (AChE) in the brain and to establish a method for measuring the amount of binding of orally administered donepezil.

METHODS

[5-^{11}C-methoxy]-donepezil ([^{11}C]-donepezil) was radiolabelled as a positron emission tomography (PET) tracer. The biodistribution of [^{11}C]-donepezil was measured by PET in 10 AD patients and six elderly normal subjects. Two AD patients underwent additional PET measurements after oral administration of donepezil for 6 months.

RESULTS

[^{11}C]-donepezil-PET images demonstrated high densities of tracer distribution in AChE-rich brain regions such as the striatum, thalamus, and cerebellum. Compared with elderly normal subjects, patients with mild AD exhibited about 18–20% reduction of donepezil binding in the neocortex and hippocampus, while patients with moderate AD exhibited about 24–30% reduction of donepezil binding throughout the brain. Orally administered donepezil (5 mg day^{-1}) induced 61.6–63.3% reduction of donepezil binding in AD brains. The distribution volume of [^{11}C]-donepezil in the hippocampus was significantly correlated with MMSE scores in AD patients.

CONCLUSIONS

[^{11}C]-donepezil-PET enables quantitative measurement of donepezil binding in the brain. AD patients exhibited reduction of donepezil binding in the brain, even in the early stage of disease. Longitudinal evaluation by this technique enables determination of AChE binding occupancy of orally administered donepezil.

Introduction

Cholinergic deficit is consistently found in the brain of patients with Alzheimer's disease (AD). Reduction in the activity of choline acetyltransferase (ChAT) and acetylcholinesterase (AChE) is evident in AD brains and correlates with cognitive decline [1, 2]. For this reason, cholinergic enhancement is a major approach to the treatment of AD. Currently, several AChE inhibitors (AChEIs) are widely prescribed to improve cognitive function in patients with AD [3]. However, not all patients respond to these treatments. It is thus important to identify factors that determine individual responses to treatment with AChEIs.

Functional imaging of cholinergic function is a useful strategy for determination of the treatment protocol of demented patients. Use of AChEIs themselves as radiotracers enables direct investigation of the pharmacokinetics of AChEIs using positron emission tomography (PET). Donepezil hydrochloride is currently the AChEI most widely used for the treatment of AD. It exhibits selective binding of AChE compared with butyrylcholinesterase (BuChE) [4]. Radiolabelled donepezil can thus be used as a tracer to measure brain concentrations of AChE. If the distribution of donepezil in the brain can be measured quantitatively by PET, this will be useful for pharmacological evaluation of AChEIs and for prediction of efficacy of treatment with donepezil. In this study, we performed PET examinations using [5-^{11}C-methoxy]-donepezil ([^{11}C]-donepezil) and determined the *in vivo* binding characteristics of donepezil in AD patients.

Methods

Subjects and patients

Six elderly normal subjects and 10 patients with probable AD were studied to examine the distribution of [^{11}C]-donepezil in the brain. The AD patients were recruited through The Tohoku University Hospital Dementia Patients Registry. The diagnosis of AD was made according to the National Institute of Neurologic Disorders and Stroke/Alzheimer's Disease and Related Disorders Association (NINCDS-ADRDA) criteria. AD patients were further divided into two groups by severity: a mild AD group ($n = 5$; MMSE score ≥ 23 points) and a moderate AD group ($n = 5$; MMSE score < 20 points). The normal control group was comprised of volunteers without impairment of cognitive function who had no cerebrovascular lesions on magnetic resonance (MR) images. After complete description of the study to the patients and subjects, written informed consent was obtained from them. PET study was performed within 3 months after the completion of a medical and neuropsychological examination. Although no significant difference in age was observed between the mild AD group and elderly normal group, the moderate AD group was older than the elderly normal group (Table 1). The MMSE score of the elderly normal subjects (mean ± SD 29.7 ± 0.8) was significantly higher than that of the mild AD (25.0 ± 1.6) and moderate AD (15.4 ± 2.7) subjects.

Table 1

Subjects and patients demographics

		Gender	Age	MMSE
Elderly normal	AN1	M	64	30
	AN2	M	61	30
	AN3	F	59	30
	AN4	F	60	30
	AN5	M	74	28
	AN6	F	75	30
	Mean		65.5	29.7
	SD		7.2	0.8
Mild AD	AD1	F	77	24
	AD2	F	72	23
	AD3	M	71	26
	AD4	F	66	25
	AD5	M	69	27
	Mean		71.0	25.0
	SD		4.1	1.6
Moderate AD	AD6	F	77	14
	AD7	F	78	12
	AD8	F	79	19
	AD9	M	84	17
	AD10	F	81	15
	Mean		79.8	15.4
	SD		2.8	2.7

Radiosynthesis of [5-^{11}C-methoxy]-donepezil

Synthesis of [^{11}C]-donepezil was performed (Figure 1) as described previously [5]. Briefly, 5′-O-desmethylprecursor (M2) was dissolved in methylethylketone and then tetrabutylammonium hydroxide was added. [^{11}C]-Methyl iodide was prepared from [^{11}C]-CO_2 and converted to [^{11}C]-methyl triflate ([^{11}C]-MeOTf). [^{11}C]-Donepezil was produced on the loop from [^{11}C]-MeOTf and purified by high performance liquid chromatography (HPLC). The radioactivity obtained was 155.4–814 MBq (4.2–22 mCi), and the radiochemical yield was 25–30% based on [^{11}C]-MeOTf after decay-correction. Specific activity was 111–354 GBq μmol^{-1} at the end of synthesis (30–40 min from the end of ^{11}C production). Radiochemical purity was greater than 99%.

PET acquisition protocols

The protocol of the PET study was approved by the Committee on Clinical Investigation at The Tohoku University School of Medicine and the Advisory Committee on Radioactive Substances at Tohoku University. The [^{11}C]-donepezil PET study was performed using a SET-2400 W PET scanner (Shimadzu Inc., Japan) under resting condition with eyes closed. Following a ^{68}Ge/Ga transmission scan of 7 min duration, an emission scan was started soon after intravenous injection of 7.1–9.5 mCi of [^{11}C]-donepezil. Emission

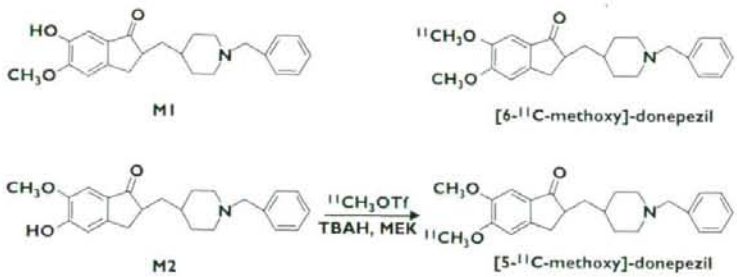

Figure 1

Chemical structures and radiosynthesis of donepezil and its metabolites

data were acquired for 60 min. Standardized uptake value (SUV) images were obtained by normalizing tissue concentration by injected dose and body mass. Arterialized venous blood samples were obtained from a hand vein, heated in a far-infrared mat, and radioactivity was measured in a well-type scintillation counter. Sampled plasma (2 ml) was denaturated with 1 M $HClO_4$: MeCN (7 : 3) and centrifuged at 3000 × *g* for 3 min. The supernatant solution was injected into a column (YMC ODS A-324, YMC Co., Ltd, Kyoto, Japan; 10 mm i.d. × 30 cm long) with a solvent system of 0.1 M ammonium formate : acetonitrile (60 : 40) at a flow rate of 5.0 ml min^{-1}. The eluates were collected at time intervals of 0.5 min and were counted for radioactivity with a gamma counter.

Image analysis

Region of interest (ROI) analysis was performed to evaluate the regional distribution of [^{11}C]-donepezil. Circular ROIs (1.0 cm in diameter) were placed on individual axial PET images in the cerebellar hemisphere, striatum, thalamus, lateral frontal cortex (Brodmann's areas (BA) 44, 45, 46, and 47), lateral temporal cortex (BA 20, 21, and 22), parietal cortex (BA 39 and 40), occipital cortex (BA 17), anterior cingulate cortex (BA 24 and 32), posterior cingulate cortex (BA 23 and 31), and medial temporal cortex (BA 27, 28, 34, and 35), referring to the individual MR images. To measure donepezil -binding AChE density in the brain, the distribution volume (DV), the ratio of [^{11}C]-donepezil concentration in tissue to that in plasma at equilibrium, was calculated by Logan's graphical analysis [6], since donepezil reversibly binds to AChE. Using this method, the DV in each ROI was determined from the slopes obtained from the values of each ROI and input function from metabolite-corrected plasma radioactivity. The slopes were determined from the last 15 points of the respective regions. Details of the quantitative analysis will be described elsewhere.

Statistical analysis

Differences in age, MMSE score, and DV among the three groups were evaluated by one-way analysis of variance (ANOVA) followed by Bonferroni's multiple comparison test (GraphPad Prism Software). For each analysis, findings were considered significant at $P < 0.05$.

Results

Tissue time activity curves (TAC) of [^{11}C]-donepezil in the brain indicated initial rapid uptake of radioactivity followed by gradual clearance from the brain in both elderly normal (Figure 2A) and AD subjects (Figure 2B). Relatively high concentrations of radioactivity of [^{11}C]-donepezil were observed in AChE-rich brain regions such as the striatum, thalamus, and cerebellum, whereas radioactivity uptake in the neocortex including frontal, temporal, and parietal cortices was moderate. Plasma radioactivity of [^{11}C]-donepezil peaked at 30–60 s postinjection, followed by a rapid decline (Figure 2C). Proportions of unchanged [^{11}C]-donepezil in plasma were 91.0 ± 7.0%, 88.1 ± 12.5%, and 82.5 ± 5.1% at 5, 15, and 30 min postinjection, respectively. The metabolite-corrected plasma time–activity curve was used to calculate specific DVs from the region-of-interest-derived regional time–activity curve. [^{11}C]-donepezil exhibited linear regression curves on Logan plot analysis in all brain regions examined (Figure 3). Since the slopes of the regression lines represent the DV of the tracer, these findings indicate a higher DV of donepezil in the striatum than in the frontal cortex. Parametric images of [^{11}C]-donepezil DV clearly revealed higher concentrations of tracer distribution in the striatum and cerebellum than in the neocortex. Patients with mild AD exhibited reduction of DV in the hippocampus and neocortex, compared with elderly normal subjects. The magnitude of DV reduction in the mild AD group was about 20% in the hippocampus and 18% in temporal and parietal cortices. In patients with moderate AD, DV reduction was evident throughout the brain (Figure 4, Figure 5, Table 2). The magnitude of DV reduction was about 30% in the hippocampus and 24% in frontal, temporal, and parietal cortices. Two AD patients (AD3 and AD10) underwent another PET scan after treatment with 5 mg donepezil for 6 months. Orally

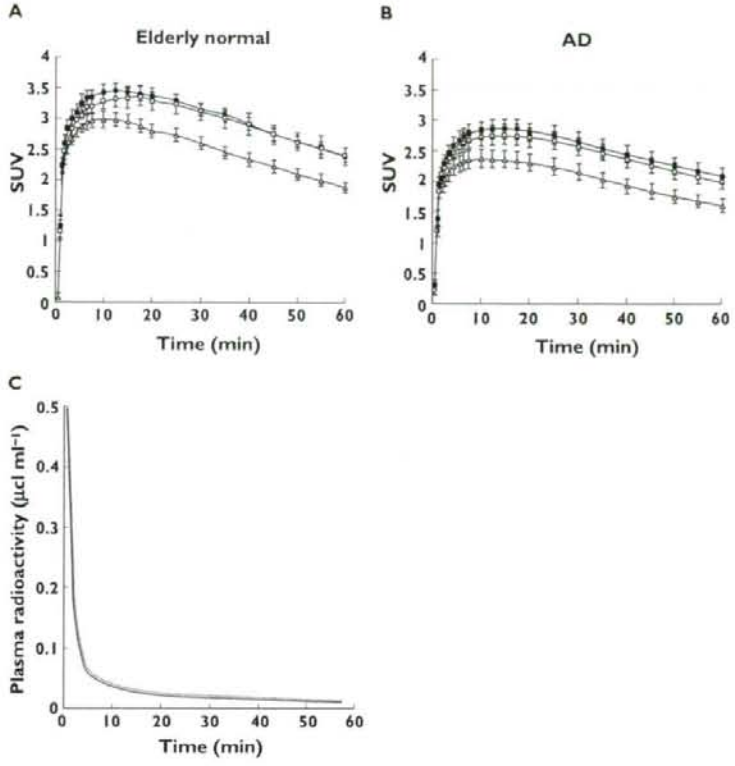

Figure 2

Time activity data for [^{11}C]-donepezil PET in humans. Brain SUV time activity curves for elderly normal subjects (A) and AD patients (B), and plasma time activity curve (C) are shown. The dotted line indicates total time activity curve and the solid line indicates metabolite-corrected time activity curve

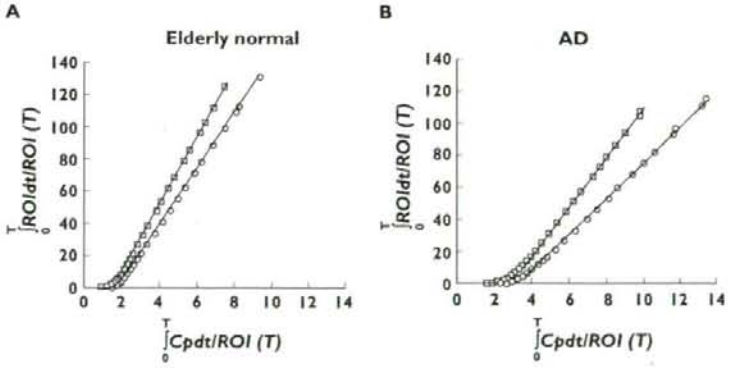

Figure 3

Logan plots for the striatum (□) and frontal cortex (○) for elderly normal subjects (A) and AD patients (B). *Cp*: plasma concentration of tracer, ROI: region of interest, *T*: time after injection

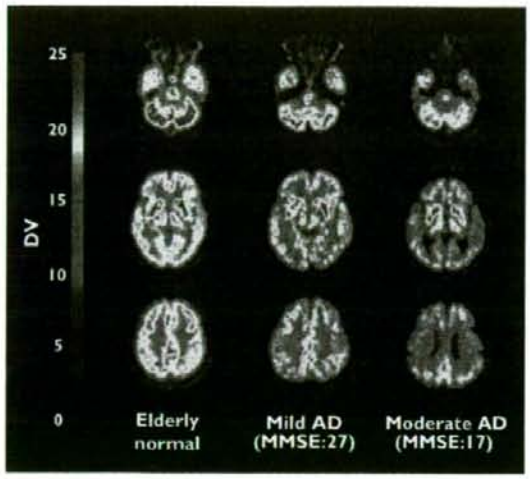

Figure 4

Distribution volume images of [^{11}C]-donepezil in elderly normal subjects (left), patients with mild AD (middle), and patients with moderate AD (right)

administered donepezil induced substantial reduction of DV in all regions of brain examined (Figure 6). Mean DV reduction in patient 1 (AD3) was 61.6% (55.5% in the cerebellum, 65.2% in the striatum, 63.6% in the thalamus, 62.5% in the frontal cortex, 61.6% in the temporal cortex, 59.6% in the parietal cortex, 62.6% in the occipital cortex, 60.3% in the anterior cingulate cortex, 59.5% in the posterior cingulate cortex and 65.5% in the medial temporal cortex). Mean DV reduction in patient 2 (AD10) was 63.3% (59.9% in the cerebellum, 72.0% in the striatum, 60.6% in the thalamus, 61.6% in the frontal cortex, 62.9% in the temporal cortex, 62.4% in the parietal cortex, 54.2% in the occipital cortex, 62.4% in the anterior cingulate cortex, 57.9% in the posterior cingulate cortex and 78.8% in medial temporal cortex). Finally, the correlation of donepezil binding with severity of dementia was examined within the AD patient group. As shown in Figure 7, the DV value in the hippocampus was significantly correlated with MMSE scores of AD patients.

Discussion

Currently, *in vivo* monitoring of brain AChE activity using positron emission tomography (PET) is beneficial in developing strategies for dementia therapy. [^{11}C]-MP4A and [^{11}C]-PMP, which are metabolically trapped acetylcholine analogues, have been successfully applied to the evaluation of AChE activity in the brain [7, 8]. PET studies in AD patients have demonstrated reduction of AChE activity in the early stage of disease, with the degree of reduction correlating with cognitive dysfunction [9, 10]. Another strategy involves use of AChEIs themselves as radiotracers. This method enables direct investigation of the pharmacokinetics of AChEIs. [^{11}C]-physostigmine [11], [^{11}C]-methyltacrine [12], and [^{11}C]-CP-126 998 [13] have been designed as radiotracers for clinical PET study. *In vivo* imaging techniques using such radiotracers can measure the concentrations of tracer-binding AChE. If these radiotracers and therapeutic drugs competitively bind to AChE, the occupancy of binding sites on AChE by therapeutic drugs could be measured by subtraction of post-treatment from pretreatment PET scans.

This PET study demonstrated that intravenously administered [^{11}C]-donepezil rapidly enters the brain and is mainly distributed in the striatum, thalamus, and cerebellum, which are known to contain high densities of AChE compared with the cerebral cortex and hippocampus. This finding is consistent with the findings of our previous study in rats [5]. The regional distribution of [^{11}C]-donepezil was also consistent with regional AChE activity determined in a human postmortem study [14], suggesting selective binding of donepezil to AChE.

Post-treatment evaluation following administration of 5 mg donepezil day^{-1} revealed a remarkable reduction (61.6–63.3% compared with pretreatment scan) of [^{11}C]-donepezil binding throughout the brain. This indicates that the AChE occupancy by donepezil, when administered in daily doses of 5 mg, was about 35–40% in these two patients. A previous PET study using [^{11}C]-MP4A revealed a mean 39% reduction in AChE activity after oral administration of 3–5 mg donepezil [15]. Intravenous administration of donepezil in monkeys also resulted in a mean 27% reduction of AChE activity at a dose of 100 μg kg^{-1} [16]. These findings together suggest that inhibition of AChE activity matches occupancy of AChEI binding sites. Moreover, orally administered donepezil (5 mg) induced substantial inhibition (43–62%) of the binding of another radiotracer, [^{11}C]-CP-126 998, to AChE [13]. This finding is roughly consistent with our observations. The amount of binding of orally administered donepezil to AChE is considered a key factor in determining therapeutic response. AChE binding occupancy by orally administered donepezil could be modulated by blood–brain barrier permeability, tissue distribution, metabolism, and also by AChE density in the brain. *In vivo* evaluation of AChE occupancy could thus be a powerful strategy for determining the optimal dose of donepezil. In the future, quantitative evaluation of donepezil binding sites might be used to optimize regimens of treatment with donepezil and to predict the response to treatment. To this purpose, red blood cell AChE inhibition has been explored as a peripheral surrogate marker for the activity of AChEIs [17]. In a future study, we plan to examine the relationship between red blood cell AChE inhibition and [^{11}C]-donepezil binding in the brain.

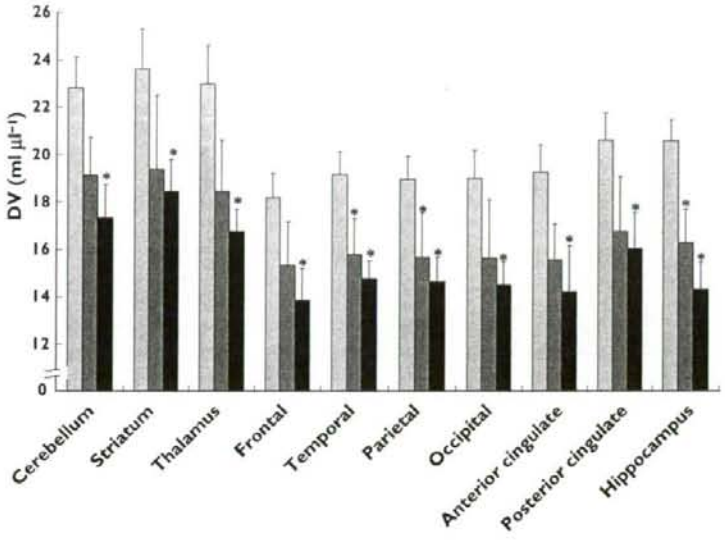

Figure 5

Regional distribution volume data in elderly normal subjects (□), mild AD (▩), and moderate AD patients (■)

Table 2

Regional distribution volume of [^{11}C]-donepezil in elderly normal subjects and AD patients (mean ± SEM)

	Elderly normal	Mild AD	Moderate AD
Cerebellum	23.4 ± 3.5	19.6 ± 1.4	17.6 ± 1.4*
Striatum	24.0 ± 4.1	20.0 ± 3.1	18.5 ± 1.6*
Thalamus	23.4 ± 4.1	19.0 ± 2.1	17.1 ± 1.0*
Frontal	18.5 ± 2.5	15.8 ± 1.8	14.0 ± 1.5*
Temporal	19.7 ± 2.6	16.2 ± 1.3*	15.1 ± 0.9*
Parietal	19.5 ± 2.7	16.1 ± 1.7*	15.0 ± 1.1*
Occipital	19.4 ± 3.2	16.1 ± 2.3	14.6 ± 1.1*
Anterior cingulate	19.6 ± 2.6	16.2 ± 1.7	14.7 ± 1.9*
Posterior cingulate	21.1 ± 3.0	17.2 ± 2.3	16.3 ± 1.7*
Hippocampus	21.4 ± 2.1	17.3 ± 2.1*	14.8 ± 1.2*

*P < 0.05, significantly different from aged normal group.

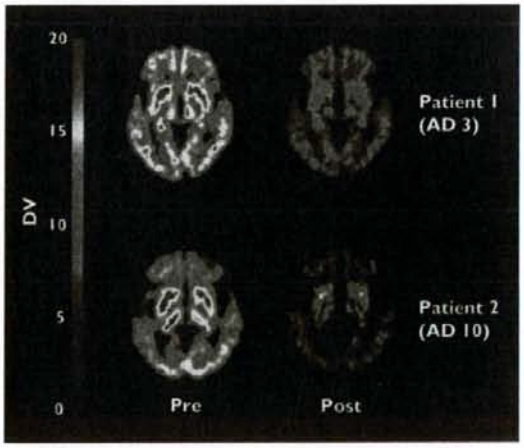

Figure 6

Distribution volume images before and after oral administration of donepezil in AD patients

Patients with moderate AD exhibited significant reduction of [^{11}C]-donepezil DV in all brain regions examined, in comparison with elderly normal subjects. Furthermore, temporo-parietal and hippocampal DVs were significantly reduced even in patients with mild AD, compared with elderly normal group. These reductions suggest early involvement of the cholinergic system in AD, since the AChE in brain is predominantly located in presynaptic cholinergic neurones [18]. A previous [^{11}C]-MP4A PET study demonstrated 21% reduction of hippocampal AChE activity in patients with early onset AD [19]. We observed an approximately 20% reduction in hippocampal DV in the mild AD group and 30% reduction in the moderate AD group. These findings suggest that the concentration of donepezil-binding AChE is matched by regional AChE activity. In a postmortem study, AD patients exhibited reduction of AChE activity, and this reduction was correlated with the severity of dementia [20, 21]. We observed

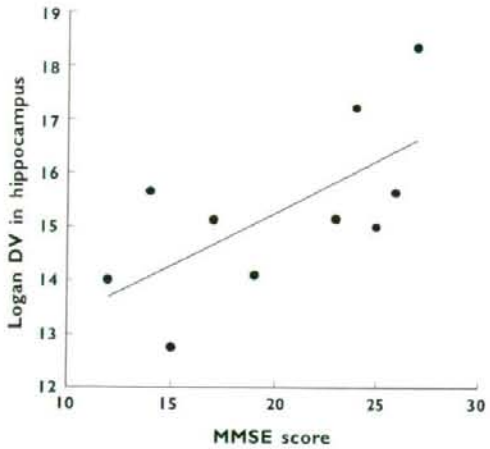

Figure 7

Correlation between MMSE scores and distribution volume in the hippocampus of AD patients. Pearson $r = 0.659$ and $p = 0.038$

that DV in the hippocampus was correlated with the cognitive status in AD patients, a finding in accord with postmortem data. However, it is important to note that the partial volume effect due to structural atrophy might cause the underestimation of DV in the hippocampus. Analysis after partial volume correction is therefore needed to establish further the relationship between the regional DV of [^{11}C]-donepezil and the severity of dementia in AD.

Compared with previously reported findings of PET imaging with [^{11}C]-MP4A [9] and [^{11}C]-PMP [10], the present [^{11}C]-donepezil-PET study demonstrated a relatively higher cortical retention of radiotracer, suggesting the existence of alternative binding sites for donepezil other than AChE. Donepezil is reported to have high binding affinity for σ_1-receptors, which are widely distributed in the brain including the cerebral cortex, hippocampus, and cerebellum [22–24]. A recent human PET study using a σ_1-receptor-specific radioligand demonstrated prominent reduction of σ_1-receptor density in the cerebral cortex and cerebellum of AD patients [25]. Thus, concomitant binding of donepezil to σ_1-receptors might have contributed to the distinctive distribution of [^{11}C]-donepezil we observed in the brain.

Previously, the tracer kinetics of [^{11}C]-donepezil with labelling of the methoxy group at position 6 ([6-^{11}C-methoxy]-donepezil) were examined in mice and rabbits, to test this agent as a candidate for a PET radioligand [26]. However, the regional brain distribution of this radiotracer did not reflect the distribution of AChE in the brain. In contrast, our previous study yielded successful *in vivo* visualization of AChE by donepezil labelled with ^{11}C at the methoxy group at position 5 ([5-^{11}C-methoxy]-donepezil) [5]. The differences between these findings might be attributable to the affinity of unlabelled metabolites to AChE. Indeed, the unlabelled metabolite of [6-^{11}C-methoxy]-donepezil (M1 in Figure 1) has high binding affinity for AChE ($IC_{50} = 6.4$ nM), resulting in competition for binding between ^{11}C-labelled tracer and unlabelled metabolite, while the metabolite of [5-^{11}C-methoxy]-donepezil (M2 in Figure 1) exhibits lower affinity of binding to AChE ($IC_{50} = 1.1$ μM) than M1. [5-^{11}C-methoxy]-donepezil is thus suitable for detection of AChE *in vivo*. In addition, the specific radioactivity of [5-^{11}C-methoxy]-donepezil in this study (111–354 GBq μmol^{-1}) was higher than that of [6-^{11}C-methoxy]-donepezil in a previous study [26]. High specific activity of [^{11}C]-donepezil might therefore be another contributing factor of successful visualization of AChE.

In this study, the distribution of donepezil in human brain was successfully visualized using [^{11}C]-donepezil and PET. Graphical analysis by Logan plots can be used to obtain quantitative estimates of specific donepezil binding. AD patients exhibited significant reduction of donepezil distribution, even in the early stages of disease. This imaging technique will be useful as a new surrogate marker for evaluation of treatment with donepezil.

This work was in part supported by Grants-in-Aid for scientific research (No. 17390156 for K.Yanai and 18019004 for N. Okamura) from the Japan Society of Promotion of Science (JSPS) and the Ministry of Education, Culture, Sports, Science and Technology in Japan, as well as by a grant from the Japan Society of Technology (JST) on research and education in 'molecular imaging'. The authors thank the volunteers, Dr Syoichi Watanuki for PET operation and Mrs Kazuko Takeda for taking care of the volunteers.

REFERENCES

1 Davies P, Maloney AJ. Selective loss of central cholinergic neurons in Alzheimer's disease. Lancet 1976; 2: 1403.

2 Coyle JT, Price DL, DeLong MR. Alzheimer's disease: a disorder of cortical cholinergic innervation. Science 1983; 219: 1184–90.

3 Giacobini E. Cholinesterase inhibitors: from the Calabar bean to Alzheimer therapy. In: Cholinesterases and Cholinesterase Inhibitors, ed. Giacobini E. London: 2000.

4 Sugimoto H, Ogura H, Arai Y, Iimura Y, Yamanishi Y. Research and development of donepezil hydrochloride, a new type of acetylcholinesterase inhibitor. Jpn J Pharmacol 2002; 89: 7–20.

5 Funaki Y, Kato M, Iwata R, Sakurai E, Sakurai E, Tashiro M, Ido T, Yanai K. Evaluation of the binding characteristics of [5-(11) C-methoxy]-donepezil in the rat brain for *in vivo* visualization of acetylcholinesterase. J Pharmacol Sci 2003; 91: 105–12.

6 Logan J. Graphical analysis of PET data applied to reversible and irreversible tracers. Nucl Med Biol 2000; 27: 661–70.

7 Kilbourn MR, Snyder SE, Sherman PS, Kuhl DE. *In vivo* studies of acetylcholinesterase activity using a labeled substrate, N-[^{11}C]methylpiperdin-4-yl propionate ([^{11}C]PMP). Synapse 1996; 22: 123–31.

8 Irie T, Fukushi K, Namba H, Iyo M, Tamagami H, Nagatsuka S, Ikota N. Brain acetylcholinesterase activity: validation of a PET tracer in a rat model of Alzheimer's disease. J Nucl Med 1996; 37: 649–55.

9 Iyo M, Namba H, Fukushi K, Shinotoh H, Nagatsuka S, Suhara T, Sudo Y, Suzuki K, Irie T. Measurement of acetylcholinesterase by positron emission tomography in the brains of healthy controls and patients with Alzheimer's disease. Lancet 1997; 349: 1805–9.

10 Kuhl DE, Koeppe RA, Minoshima S, Snyder SE, Ficaro EP, Foster NL, Frey KA, Kilbourn MR. *In vivo* mapping of cerebral acetylcholinesterase activity in aging and Alzheimer's disease. Neurology 1999; 52: 691–9.

11 Blomqvist G, Tavitian B, Pappata S, Crouzel C, Jobert A, Doignon I, Di Giamberardino L. Quantitative measurement of cerebral acetylcholinesterase using [^{11}C]physostigmine and positron emission tomography. J Cereb Blood Flow Metab 2001; 21: 114–31.

12 Tavitian B, Pappata S, Bonnot-Lours S, Prenant C, Jobert A, Crouzel C, Di Giamberardino L. Positron emission tomography study of [^{11}C]methyl-tetrahydroaminoacridine (methyl-tacrine) in baboon brain. Eur J Pharmacol 1993; 236: 229–38.

13 Bencherif B, Endres CJ, Musachio JL, Villalobos A, Hilton J, Scheffel U, Dannals RF, Williams S, Frost JJ. PET imaging of brain acetylcholinesterase using [^{11}C]CP-126 998, a brain selective enzyme inhibitor. Synapse 2002; 45: 1–9.

14 Finkelstein Y, Wolff M, Biegon A. Brain acetylcholinesterase after acute parathion poisoning: a comparative quantitative histochemical analysis post mortem. Ann Neurol 1988; 24: 252–7.

15 Shinotoh H, Aotsuka A, Fukushi K, Nagatsuka S, Tanaka N, Ota T, Tanada S, Irie T. Effect of donepezil on brain acetylcholinesterase activity in patients with AD measured by PET. Neurology 2001; 56: 408–10.

16 Shiraishi T, Kikuchi T, Fukushi K, Shinotoh H, Nagatsuka S, Tanaka N, Ota T, Sato K, Hirano S, Tanada S, Iyo M, Irie T. Estimation of plasma IC_{50} of donepezil hydrochloride for brain acetylcholinesterase inhibition in monkey using N-[^{11}C]methylpiperidin-4-yl acetate ([^{11}C]MP4A) and PET. Neuropsychopharmacology 2005; 30: 2154–61.

17 Sramek JJ, Cutler NR. RBC cholinesterase inhibition: a useful surrogate marker for cholinesterase inhibitor activity in Alzheimer disease therapy? Alzheimer Dis Assoc Disord 2000; 14: 216–27.

18 Mesulam MM, Geula C. Overlap between acetylcholinesterase-rich and choline acetyltransferase-positive (cholinergic) axons in human cerebral cortex. Brain Res 1992; 577: 112–20.

19 Shinotoh H, Namba H, Fukushi K, Nagatsuka S, Tanaka N, Aotsuka A, Ota T, Tanada S, Irie T. Progressive loss of cortical acetylcholinesterase activity in association with cognitive decline in Alzheimer's disease: a positron emission tomography study. Ann Neurol 2000; 48: 194–200.

20 Zubenko GS, Moossy J, Martinez AJ, Rao GR, Kopp U, Hanin I. A brain regional analysis of morphologic and cholinergic abnormalities in Alzheimer's disease. Arch Neurol 1989; 46: 634–8.

21 Prohovnik I, Perl DP, Davis KL, Libow L, Lesser G, Haroutunian V. Dissociation of neuropathology from severity of dementia in late-onset Alzheimer disease. Neurology 2006; 66: 49–55.

22 Kato K, Hayako H, Ishihara Y, Marui S, Iwane M, Miyamoto M. TAK-147, an acetylcholinesterase inhibitor, increases choline acetyltransferase activity in cultured rat septal cholinergic neurons. Neurosci Lett 1999; 260: 5–8.

23 Guitart X, Codony X, Monroy X. Sigma receptors: biology and therapeutic potential. Psychopharmacology 2004; 174: 301–19.

24 Sakata M, Kimura Y, Naganawa M, Oda K, Ishii K, Chihara K, Ishiwata K. Mapping of human cerebral sigma1 receptors using positron emission tomography and [^{11}C]SA4503. Neuroimage 2007; 35: 1–8.

25 Hashimoto K, Ishiwata K. Sigma receptor ligands: possible application as therapeutic drugs and as radiopharmaceuticals. Curr Pharm Des 2006; 12: 3857–76.

26 De Vos F, Santens P, Vermeirsch H, Dewolf I, Dumont F, Slegers G, Dierckx RA, De Reuck J. Pharmacological evaluation of [^{11}C]donepezil as a tracer for visualization of acetylcholinesterase by PET. Nucl Med Biol 2000; 27: 745–7.

Ann Nucl Med (2008) 22:151–156
DOI 10.1007/s12149-007-0094-z

ORIGINAL ARTICLE

Low density of sigma$_1$ receptors in early Alzheimer's disease

**Masahiro Mishina · Masashi Ohyama · Kenji Ishii
Shin Kitamura · Yuichi Kimura · Kei-ichi Oda
Kazunori Kawamura · Toru Sasaki · Shiro Kobayashi
Yasuo Katayama · Kiichi Ishiwata**

Received: 24 July 2007 / Accepted: 5 September 2007

Abstract
Objective The sigma$_1$ receptor is considered to be involved in cognitive function. A postmortem study reported that the sigma$_1$ receptors were reduced in the hippocampus in Alzheimer's disease (AD). However, in vivo imaging of sigma$_1$ receptors in the brain of AD patients has not been reported. The aim of this study is to investigate the mapping of sigma$_1$ receptors in AD using [^{11}C]SA4503 positron emission tomography (PET).

Methods We studied five AD patients and seven elderly volunteers. A dynamic series of decay-corrected PET data acquisition was performed for 90 min starting at the time of the injection of 500 MBq of [^{11}C]SA4503. A two-tissue three-compartment model was used to estimate K_1, k_2, k_3, k_4, and the delay between metabolite-corrected plasma and tissue time activity using a Gauss–Newton algorithm. The ratio of k_3 to k_4 was computed as the binding potential (BP), which is linearly related to the density of sigma$_1$ receptors. Unpaired t tests were used to compare K_1 and BP in patients with AD and normal subjects.
Results As compared with normals, BP in the AD was significantly lower in the frontal, temporal, and occipital lobe, cerebellum and thalamus, whereas K_1 was significantly lower in the parietal lobe.
Conclusions [^{11}C]SA4503 PET can demonstrate that the density of cerebral and cerebellar sigma$_1$ receptors is reduced in early AD.

Keywords Alzheimer's disease · Positron emission tomography · Sigma$_1$ receptor · Cortex · Cerebellum

M. Mishina · M. Ohyama · K. Ishii · Y. Kimura · K. Oda · K. Kawamura · T. Sasaki · K. Ishiwata
Positron Medical Center, Tokyo Metropolitan Institute of Gerontology, Tokyo, Japan

M. Mishina · M. Ohyama · S. Kitamura · Y. Katayama
Department of Neurology, Nephrology and Rheumatology, Nippon Medical School, Tokyo, Japan

M. Mishina (✉) · S. Kobayashi
Neurological Institute, Nippon Medical School Chiba-Hokusoh Hospital, 1715 Kamagari, Imba-mura, Imba-gun, Chiba 270-1694, Japan
e-mail: mishina@nms.ac.jp

S. Kitamura
Department of Internal Medicine, Nippon Medical School Musashi Kosugi Hospital, Kanagawa, Japan

Y. Kimura
Biophysics Group, Molecular Imaging Center, National Institute of Radiological Sciences, Chiba, Japan

K. Kawamura
Center for Integrated Brain Science, Brain Research Institute, University of Niigata, Niigata, Japan

T. Sasaki
Research Team for Molecular Biomarkers, Tokyo Metropolitan Institute of Gerontology, Tokyo, Japan

Introduction

Sigma$_1$ receptor has received considerable attention in the regulation of cognitive function [1]. The sigma receptor has been established as a distinct receptor, although it was initially proposed as a subtype of opioid receptors [2]. It is classified into at least two subtypes, namely, sigma$_1$ and sigma$_2$ [3]. Although an endogenous ligand for the sigma receptors remains unclear, some studies have reported that steroid hormones such as progesterone and testosterone might interact with sigma

receptors [4, 5]. Confirmed sigma$_1$ receptor ligand functions are neuro-protective, anti-depressant, and anti-amnestic functions [6, 7]. Sigma$_1$ receptor agonists improved impairment of learning and memory in mice [8–10]. Matsuno et al. [11–13] showed that the sigma$_1$ receptor agonists such as (+)-SKF-10,047 and SA4503 increased extracellular acetylcholine levels in the rat frontal cortex and hippocampus. The sigma$_1$ receptor is considered to be involved in aging [14, 15] and various diseases, such as schizophrenia [16], depression [17], ischemia [18], and Parkinson's disease [19]. In patients with Alzheimer's disease (AD), a postmortem study showed that the sigma$_1$ binding sites were reduced in the hippocampus [20]. The sigma$_1$ receptor agonists are also expected as drugs for improving the cognitive deficits of AD [21]. However, the distribution of sigma$_1$ receptors in patients with AD remains to be determined. We developed a positron emission tomography (PET) ligand, [^{11}C]SA4503 (Fig. 1), for mapping the sigma$_1$ receptors [22–24], and reported that sigma$_1$ receptor was down-regulated in the putamen with Parkinson's disease [19]. The objective of this study was to investigate the change of sigma$_1$ receptor in the early phase of AD using [^{11}C]SA4503 PET.

Materials and methods

Subjects

We studied five patients (two men and three women, mean age ± SD, 74.6 ± 3.2 years) diagnosed as having probable AD on the basis of the National Institute of Neurological and Communicative Diseases and Stroke/Alzheimer's Disease and Related Disorders Association (NINCDS–ADRDA) criteria [25]. Magnetic resonance imaging (MRI) scans were obtained with a MAGNEX 1.5-T machine (Shimadzu, Kyoto, Japan) in the First Hospital of Nippon Medical School, and we confirmed that they had no diseases other than AD including stroke and brain tumor. To ensure the early diagnosis of AD, each patient was also examined for glucose metabolism by PET using [^{18}F]fluorodeoxyglucose ([^{18}F]FDG), and we confirmed hypometabolism of glucose in the temporoparietal lobe and posterior cingulate of all patients [26, 27]. The clinical severity of AD was scored in each patient according to the Functional Assessment of Staging [28], Mini-Mental State examination [29], and Clinical Dementia Rating [30] just before the [^{18}F]FDG PET examination.

The control group consisted of seven volunteers (two men and four women, age ± SD 62.6 ± 8.2), without any history of neurological diseases or abnormalities on physical or neurological examinations. MRI scans were obtained with a SIGNA 1.5-T machine (General Electric, WI, USA) in the Tokyo Metropolitan Geriatric Hospital for the normal subjects, and we confirmed that they had no neurological diseases, such as stroke and brain tumor. They were not currently receiving medications known to affect brain metabolism. None had a history of alcoholism.

The Ethics Committee of Tokyo Metropolitan Institute of Gerontology approved this study protocol. Informed consent in writing was obtained from all of the subjects who participated in this study.

[^{11}C]SA4503 PET

Positron emission tomography was performed in the Tokyo Metropolitan Institute of Gerontology Positron Medical Center with an SET2400 W scanner (Shimadzu, Kyoto, Japan) [31]. [^{11}C]SA4503 was prepared as described earlier [23]. The specific activity at the time of injection ranged from 23.7 GBq/μmol to 130.2 GBq/μmol (72.3 ± 34.3 GBq/μmol). The transmission data were acquired with a rotating ^{68}Ga/^{68}Ge rod source for attenuation correction. A dynamic series of decay-corrected PET data acquisition was performed in the 2D mode for 90 min starting at the time of the injection of 500 MBq of [^{11}C]SA4503. Arterial blood was sampled at 10 s, 20 s, 30 s, 40 s, 50 s, 60 s, 70 s, 80 s, 90 s, 100 s, 110 s, 120 s, 135 s, and 150 s, and at 3 min, 5 min, 7 min, 10 min, 15 min, 20 min, 30 min, 40 min, 50 min, 60 min, 75 min, and 90 min. Plasma was separated, weighed, and measured for radioactivity with an NaI (Tl) well scintillation counter. Metabolite analysis was carried out by high-performance liquid chromatography [23].

Data analysis

Image manipulations were carried out on an O2 workstation (Silicon Graphics, Mountain View, CA, USA), using a medical image processing application package "Dr. View" version 5.2 (AJS, Tokyo, Japan).

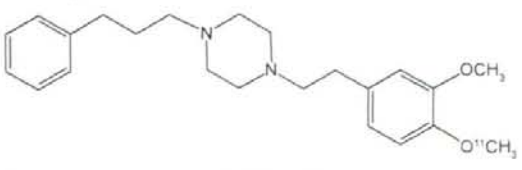

Fig. 1 Chemical structure of [^{11}C]SA4503

For [^{11}C]SA4503 PET, we generated early images for each subject by adding up the frames of the dynamic scan from 0 min to 10 min [32]. Circular regions of interest (ROIs) 10 mm in diameter and extending over two slices of the images were drawn on the cerebellum, medial temporal lobe (included hippocampus), frontal lobe, temporal lobe, occipital lobe, parietal lobe, post cingulate gyrus, thalamus, and striatum. The time course of the tissue concentration of [^{11}C]SA4503 was computed from the PET data and the interpolated ROIs throughout the scanning period. A two-tissue three-compartment model was used to estimate K_1, k_2, k_3, k_4, and the delay between metabolite-corrected plasma and tissue time activity using a Gauss–Newton algorithm [15]. The ratio of k_3 to k_4 was computed as the binding potential (BP), which is linearly related to the density of sigma$_1$ receptors. Parametric images of total distribution volume (DVt) for [^{11}C]SA4503 were also generated using a graphical analysis [33].

Statistics

Unpaired t tests were used to compare the BP in patients with AD and normal subjects. The Bonferroni correction was applied for multiple comparisons (nine comparisons corresponding to nine regions). The level of significance was set at $P < 0.05$. The statistical computation was performed using a software package "JMP" version 5.1.2 (SAS Institute, Cary, NC, USA) on a Macintosh computer.

Results

Table 1 summarizes the clinical profiles. Their average duration of illness was 2.0 ± 0.7 years. The severity of cognitive dysfunction as assessed with the Mini-Mental State examination ranged from 16 to 25.

In the ROI-based analysis, K_1 for [^{11}C]SA4503 was significantly lower in the parietal lobe of the AD patients than in that of normals, whereas there was no significant difference in other regions between AD patients and the normals (Table 2). On the other hand, BP for [^{11}C]SA4503 was significantly lower in the frontal, temporal, and occipital lobes, cerebellum and thalamus of the AD patients than in that of normals (Table 2). We also observed that BP also showed a tendency to decline in other regions of AD. Figure 2 shows representative PET images for a normal subject and a patient with AD. The DVt image demonstrates that the sigma$_1$ receptors are lower in the entire brain of the patient with AD than in that of the normal subject.

Discussion

[^{11}C]SA4503 PET demonstrated that the distribution of cortical sigma$_1$ receptors was reduced in the early phase of AD. Only in the parietal lobe could we observe a significant reduction of K_1, which was linearly related to the cerebral blood flow. The age of the control subjects was slightly younger than that of the patient group. However,

Table 1 Demographic and clinical data for patients with Alzheimer's disease (AD)

No.	Age (years)	Sex	Duration (year)	Medication before PET	FAST	MMS	CDR
1	79	M	3	Donepezil	3	25	1
2	76	M	2	Donepezil	3	21	1
3	75	F	1	Donepezil	4	16	1
4	71	F	2	None	3	17	1
5	72	F	2	None	3	22	1

PET positron emission tomography, *FAST* functional assessment of staging, *MMS* Mini-Mental State examination, *CDR* clinical dementia rating

Table 2 Comparison of K_1 and binding potential for sigma$_1$ receptors in each region in normals and patients with AD

ROI	K_1		BP	
	Normal	AD	Normal	AD
Frontal lobe	0.50 ± 0.06	0.43 ± 0.06	16.4 ± 3.0	9.2 ± 4.5*
Temporal lobe	0.52 ± 0.07	0.44 ± 0.04	17.4 ± 3.6	8.7 ± 4.3*
Hippocampus	0.46 ± 0.06	0.42 ± 0.03	18.6 ± 3.8	12.2 ± 6.8
Occipital lobe	0.58 ± 0.07	0.50 ± 0.09	13.7 ± 2.6	5.9 ± 3.3**
Parietal lobe	0.52 ± 0.06	0.39 ± 0.06*	16.7 ± 2.6	13.6 ± 10.5
Posterior cingulate	0.62 ± 0.08	0.50 ± 0.09	15.4 ± 3.2	8.7 ± 5.4
Cerebellum	0.56 ± 0.10	0.58 ± 0.06	22.5 ± 4.8	9.0 ± 5.1**
Striatum	0.55 ± 0.07	0.57 ± 0.07	13.9 ± 2.4	8.8 ± 3.5
Thalamus	0.64 ± 0.09	0.62 ± 0.09	15.2 ± 4.7	6.9 ± 2.3*

ROI regions of interest, *BP* binding potential, *AD* Alzheimer's disease
Values are mean ± SD (normal $n = 7$, AD $n = 5$). *$P < 0.05$, **$P < 0.01$ (unpaired t test)

Fig. 2 Positron emission tomography (PET) images for a 65-year-old healthy woman (**a**), and a 71-year-old woman with Alzheimer's disease (**b**). Parametric images for the DVt of [^{11}C]SA4503 were generated using a graphical analysis. [^{11}C]SA4503 PET demonstrates that the sigma$_1$ receptors are widely distributed throughout the entire brain in a normal subject (**a**). In comparison with the normal subject, the number of sigma$_1$ receptors was decreased in the brain of the patient with Alzheimer's disease (**b**)

when the BP in the control subjects (62.6 ± 8.2 years) was compared with that in the young subjects (n = 9, 28 ± 4 years) reported earlier [24], it was found to be slightly decreased with aging without statistical significance (unpublished data) in spite of an age-dependent increase of the [^{11}C]SA4503 binding in rats and monkeys [14, 15]. The reduction of the BP in AD was much more marked compared with the BP in the aged control subjects. Therefore, the reduced sigma$_1$ receptor density in AD could not be derived from the slight difference in age between the control and patient groups. PET with [^{18}F]FDG and statistical image analysis applications such as statistical parametric mapping (SPM) and 3D stereotactic surface projections have shown that in patients with AD, the cerebral glucose metabolism is reduced in the temporal-, parietal-, posterior cingulate-, and prefrontal regions [26, 27]. We also confirmed a similar pattern in the present patients with AD by [^{18}F]FDG PET (data not shown). However, these findings did not correspond with the distribution of neuronal loss on postmortem studies [34]. In a [^{11}C]flumazenil PET study on AD, Ohyama et al. [35] showed that benzodiazepine receptor was less impaired than neuronal function assessed by the cerebral blood flow and glucose metabolism in the association-cortex. The benzodiazepine receptors are one of the gamma-aminobutyric acid type A ($GABA_A$) receptor complex. The present study indicated that sigma$_1$ receptors were affected from the early stages of AD, unlike $GABA_A$ receptors. Some articles showed that the sigma$_1$ receptor agonists increased extracellular acetylcholine levels in the rat frontal cortex and hippocampus [11, 12]. Increased acetylcholine does not directly affect the [^{11}C]SA4503 binding, because acetylcholine does not bind to sigma$_1$ receptors. However, reduction of the number of sigma$_1$ receptors may reflect the cholinergic system and cognitive function of patients with AD. Amyloid imaging by PET currently represents a potentially useful tool for the early diagnosis of pre-onset AD [36]. We have an interest in the relationship between sigma$_1$ receptor in the mild cognitive impairment stage and pre-onset stage of AD. Further studies will be needed using amyloid PET and [^{11}C]SA4503 PET.

The density of sigma$_1$ receptors in the cerebellum was significantly lower in AD than in normals, although K_1 in AD was comparable with that in normals. Although the cerebellum was formerly thought to be unaffected in AD, many studies have revealed cerebellar changes in AD patients [37–43]. A pathological study showed that the density of Purkinje cell was reduced in the cerebellum of AD, especially in the vermis [41]. Using glutamate as the neurotransmitter, the granule cells deliver an excitability signal to the dendrite of Purkinje cells. Chaki et al. [44] suggested that sigma$_1$ binding sites are involved in modulating the release of dopamine by interacting with *N*-methyl-D-aspartic acid (NMDA) receptors on dopaminergic nerve terminals. Release of dopamine is reduced in the putamen with Parkinson's disease, and sigma$_1$ receptors were down-regulated in the putamen with Parkinson's disease [19]. Sigma$_1$ receptors in the cerebellum may be involved in the modulation of glutamate receptor, as well as in the putamen.

Although we could observe a reduced density of sigma$_1$ receptors in the early phase of AD, we cannot say that [^{11}C]SA4503 PET is suitable for the early diagnosis of AD. We are obliged to force the subjects to remain still for over 100 min with their heads fixed in a PET machine and to cannulate their radial artery to sample the arterial blood. Most AD patients are not suitable for the protocol of [^{11}C]SA4503 PET. Prior to the examinations, we had to confirm whether each of the AD subjects in the current study could withstand the protocol of [^{11}C]SA4503 PET. Therefore, we are now investigating a shortened protocol for [^{11}C]SA4503 PET; 40- to 60-min PET scans without arterial blood sampling could possibly provide reliable results in the practical application, which will be described elsewhere.

Acknowledgments This work was supported by a Grant-in-Aid for Scientific Research (B) No. 13557077 from the Japan Society for the Promotion of Science. The authors thank Ms. M. Ando for taking care of the subjects undergoing PET scanning.